

# Extended Grassfire Transform on Medial Axes of 2D Shapes

Lu Liu<sup>a</sup> Erin W. Chambers<sup>b</sup> David Letscher<sup>b</sup> Tao Ju<sup>a</sup>

<sup>a</sup>*Department of Computer Science and Engineering, Washington University in St. Louis*

<sup>b</sup>*Department of Mathematics and Computer Science, Saint Louis University*

---

## Abstract

The medial axis is an important shape descriptor first introduced by Blum [2] via a grassfire burning analogy. However, the medial axes are sensitive to boundary perturbations, which calls for global shape measures to identify meaningful parts of a medial axis. On the other hand, a more compact shape representation than the medial axis, such as a “center point”, is needed in various applications ranging from shape alignment to geography. In this paper, we present a uniform approach to define a global shape measure (called *extended distance function*, or EDF) along the 2D medial axis as well as the center of a 2D shape (called *extended medial axis*, or EMA). We reveal a number of properties of the EDF and EMA that resemble those of the boundary distance function and the medial axis, and show that EDF and EMA can be generated using a fire propagation process similar to Blum’s grassfire analogy, which we call the extended grassfire transform. The EDF and EMA are demonstrated on many 2D examples, and are related to and compared with existing formulations. Finally, we demonstrate the utility of EDF and EMA in pruning medial axes, aligning shapes, and shape description.

*Key words:* medial axis, significance measure, shape center, shape description

---

## 1. Introduction

### 1.1. Motivation

The medial axis is an important shape descriptor first introduced by Blum [2]. Given a 2D shape, the medial axis is the collection of interior points with at least two closest points on the boundary. Blum uses an intuitive grassfire analogy to describe the formation of the medial axis. Suppose the shape is a field of grass with uniform density. Fire is ignited on the border of the field, and propagates inward at uniform speed. The medial axis is where the different fire fronts meet and quench. In addition, the grassfire analogy associates each point in the shape with a “burning time”, which is the distance to the shape boundary. The generation of the boundary distance function and the medial axis is sometimes called the *grassfire transform*.

Medial axes often contain branches that do not represent meaningful features, such as small boundary perturbations. As a result, much effort has been devoted to formulate *significance* measures on medial axes that identify meaningful subsets (see review in Section 2.1). While many *local* measures exist (e.g., based on distances to the boundary or closest points on the boundary), well formulated *global* measures that reflect shape properties in a larger region are

scarce.

On the other hand, an even more compact shape representation than the medial axis, such as a “center point”, is needed in certain applications. For example, registering or matching two shapes often requires an initial translation alignment, which can be established based on their center points. Also, the center point of a geographical region can be useful both for mapping drawing and for motion planning. The mostly commonly used center point definition, centroid, is often unsuitable for these applications. The centroid can easily get outside a shape, and can be unstable under transformations such as isometric deformations. Despite previous efforts (see review in Section 2.2), a characterization of the center point that is interior, stable, and uniquely defined is still lacking in the literature.

We would like to note that the higher-dimensional version of these problems - computing global shape measures over the 3D medial axis or defining “center curves” of the 3D shape - is significantly more challenging. On the other hand, a sound solution in 2D may lay the foundation for approaching these harder problems.

## 1.2. Contributions

The theoretical contributions of this paper are presenting a uniform way to define a global shape measure along the 2D medial axis as well as the center of a 2D shape, and studying their properties. Our formulations are motivated by and closely follow those of the boundary distance function and the medial axis. Intuitively, the shape measure, called the *extended distance function* (EDF), measures the radius of the longest “tube” centered at a medial axis point that fits in the shape. The shape center, called the *extended medial axis* (EMA), is where the longest fitting tubes are confined at both ends. We show that EDF and EMA are similar to the boundary distance function and the medial axis in several ways. In particular, EDF is upper semi-continuous over the medial axis and has constant gradient wherever it is continuous. Also, the EMA preserves the homotopy of the medial axis, and is a unique, interior center point for any simply connected 2D shapes.

We further show that EDF and EMA can be generated using a fire propagation process similar to and continuing from Blum’s grassfire analogy. In this extended grassfire analogy, the fire is ignited at the ends of the medial axis and propagates geodesically along the medial axis at uniform speed. The EDF at a medial axis point is the burning time of this extended grassfire, while the quench site of the fire fronts is the EMA. This analogy, which we call *extended grassfire transform*, allows us to devise a simple discrete algorithm for computing EDF and EMA over discrete approximations of the medial axis.

We demonstrate the EDF and EMA on many 2D shapes, and empirically observe that they are stable under boundary perturbations. We also compare EDF with two existing global significance measures on the medial axis, one formulated via a heuristic (the Erosion Thickness (ET) measure [15]) and one mathematically defined (the Potential Residue (PR) measure [12]). We show that EDF is closely related to ET by giving an explicit definition of ET, and demonstrate several advantages of EDF over PR in terms of analytical continuity and stability.

Finally, we show several ways in which EDF and EMA can be utilized in the realm of shape modeling. First, we introduce a new medial axis significance measure based on EDF, called *Shape Tubularity*, that measures the sharpness of protrusion, and demonstrate the advantage of combining ST with ET in medial axis pruning over using ET alone. Second, we use the EMA for translational shape alignment, and demonstrate its superiority over alignment using alternative center definitions such as centroid. Finally, we introduce a new shape signature over the boundary curve, called *Boundary Eccentricity* (BE), which robustly highlights shape extremities, and use it for shape matching.

## 2. Related works

### 2.1. Significance measures on medial axes

A variety of significance (or salience, importance, etc.) measures have been proposed for identifying portions of the medial axis that depict prominent shape features, in 2D [15] and 3D [17], which can be classified into local or global ones [14,16]. *Local* measures rate a medial axis point by the boundary geometry in its immediate neighborhood, such as the angle formed by the medial axis point and its two closest boundary points [2,7,17,9] or the Euclidean distance between the two boundary points [1,6]. However, without knowledge of the shape in a larger neighborhood, local features cannot easily distinguish between noisy features on the boundary and a meaningful shape part that is thin.

On the other hand, *global* measures capture shape properties in a larger region. Global measures are much more scarce than local ones. Shaked and Bruckstein proposed a suite of global measures over 2D medial axes using a propagation heuristic [15]. A particular notable measure formulated in their approach is the Erosion Thickness (ET) measure, which approximates the area of the 2D shape eroded in response to the loss of a skeleton branch [15]. However, an explicit definition of ET is still lacking. Ogniewicz and Ilg proposed several global measures with explicit mathematical definitions, which are based on measuring the length between the closest boundary points over the boundary curve (Potential Residue (PR)) [12]. The PR measure has been extended to evaluate 3D surface skeletons using lengths of geodesic curves on surfaces [5,14], and even further to evaluate 3D curve skeletons using approximated areas of geodesic patches [14].

### 2.2. Center points of 2D shapes

The most common way of defining a shape center is the “center of mass” or centroid, which minimizes the sum of squared Euclidean distances to all points either on the boundary of the shape or over the entire shape. However, centroid may lie outside the shape if it is non-convex, and can be unstable under large shape deformations (see discussion in Section 6.2).

In the computational geometry literature, there are a number of alternative definitions that utilize geodesic distances within the shape to prevent the center from going outside. The *geodesic center* [13] minimizes the maximum geodesic distance to any point in the shape. The *link center* [10] in a polygonal region minimizes the maximum number of straight line segments in the geodesic path to any point in the shape. The *geodesic median* [8] minimizes the average geodesic distance in the  $L_1$  norm to any point in the shape. However, these center locations may lie on the boundary (e.g., a concave vertex in a non-convex shape), and hence are not always strictly interior. Note that, among these definitions, the link center is not uniquely defined.

In geography, one way to define the center of a geographical region is the furthest point from the boundary (or center of the largest inscribed disk). Although strictly interior, such center is obviously not unique. This and other centers are compared with our extended medial axes (EMA) in a simple 2D shape in Figure 1.

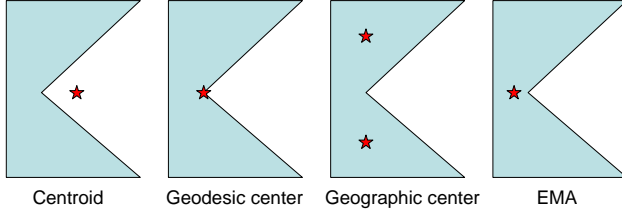


Fig. 1. Comparison of several center definitions.

Ogniewicz and Ilg [12] showed that the PR measure has a unique local maximum on the medial axis for a simply connected shape. This maximum is a unique, interior center point. However, as we demonstrate in Section 5, this local maximum can be sensitive to non-uniform boundary perturbations.

### 3. Formulation

#### 3.1. Motivation

Our definitions of the extended distance function and the extended medial axis is motivated from those of the boundary distance function and the medial axis. In a 2D shape  $O$ , the distance from an interior point  $x$  to the boundary of  $O$  can be defined as the radius of the largest circle centered at  $x$  and inscribed in  $O$ . A point is on the medial axis if its largest inscribed circle touches the boundary of  $O$  at two or more points. Due to the isotropic nature of the circle, the distance function at  $x$  captures the amount of uniform shape expansion around  $x$ , and the medial axis is where such expansion is constrained at two or more sites, and hence “maximal”.

To capture the elongation, or “side-way” expansion, of a shape around a point  $x$  on the medial axis, our extended distance function essentially measures the half-length of the longest “tube” centered at  $x$  and inscribed in  $O$ . This tube extends longitudinally along the medial axis, rather than uniformly as in the case of the circle. The extended medial axis consist of those points on the medial axis whose longest inscribed tubes are confined at both ends, and hence are where the elongation is maximal.

#### 3.2. Definitions

We assume the 2D shape  $O$  is a closed set bounded by piece-wise  $C^2$  smooth curves. The medial axis  $M$  of  $O$  are the closure of those points with two or more closest points on the boundary of  $O$  (or the “cut loci”) [18]. The regularity of the boundary implies a number of important proper-

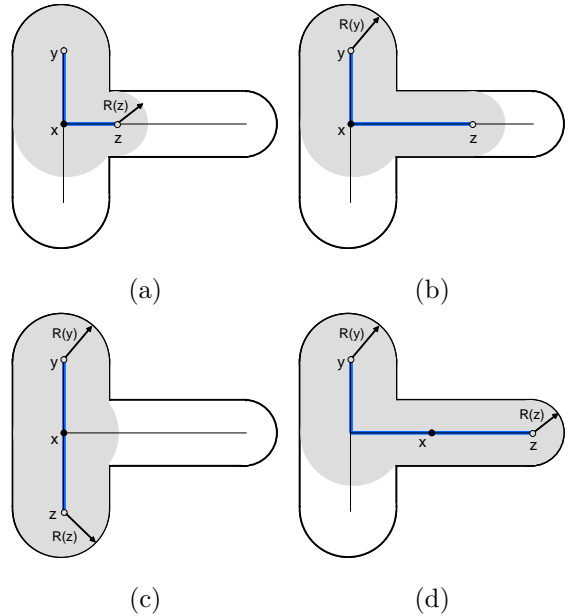


Fig. 2. Axes (blue) and their tubes (gray): (a) an axis with a single constrained end  $z$ , (b) an inscribed axis of  $x$  with a constrained end  $y$ , (c) an inscribed and maximal axis of  $x$  with two constrained ends  $y, z$ , (d) an inscribed and maximal axis of  $x \in \tilde{M}$ .

ties of  $M$ , such as its homotopy equivalence to  $O$  [18], its low-dimensionality (1) [18], and its finite structure [4]. We denote the boundary distance function at  $x \in O$  as  $R(x)$ .

We first introduce the notion of “axes” and “tubes”:

**Definition 1** Let  $f : \mathbb{R}^1 \rightarrow \mathbb{R}^2$  be a local embedding of the real interval  $D = [0, 1]$  onto  $M$ . The image  $f(D) \subseteq M$  (noted simply as  $f$  hereafter) is called an axis.

An axis is a path on  $M$  so that each interior point on the path has a manifold neighborhood. By local embedding (i.e., immersion), we allow an axis to be non-simple and hence containing loops. This relaxation is crucial to obtain some important properties later, such as the homotopy equivalence between the extended medial axis and the medial axis.

We call the union of all largest inscribed circles centered at points on an axis  $f$  the *tube* of  $f$ . Intuitively, the tube is formed by “rolling” a circle along  $f$ , while changing its radius according to the boundary distances on  $f$ . Note that when the axis is a non-simple path, the tube can “wrap around” itself.

Given some point  $x$  on an axis  $f$ , we are interested in the *radius* of  $f$  with respect to  $x$ , which is defined as the distance from  $x$  to the shorter end of the tube of  $f$ :

**Definition 2** Given an axis  $f$  and a point  $x \in f$ ,

$$r_f(x) = \min_{y \in \partial f} (d_f(x, y) + R(y))$$

is called the *radius* of  $f$  with respect to  $x$ , where  $d_f(x, y)$  is the geodesic length of segment  $[x, y]$  on  $f$ . An end  $y \in \partial f$  is called a *constrained end* with respect to  $x$  if it attains the minimum in this equation, and an *unconstrained end* otherwise.

Figure 2 (a,b,c) illustrate three different axes and their radii for a same point  $x$  on the medial axis. The first two axes each has one constrained end ( $z$  in (a) and  $y$  in (b)), where the radius of the axis is attained. The third axis has two constrained ends ( $y, z$ ) due to symmetry of the shape, both attaining the radius of the axis.

The extended distance function at  $x$  is the largest radius of any axis containing  $x$ :

**Definition 3** Given a point  $x \in M$ ,

$$\tilde{R}(x) = \sup_{f \ni x} r_f(x)$$

is called the extended distance function (EDF) at  $x$ . The axis  $f$  that attains the supremum is called the inscribed axis at  $x$ .

Intuitively, the EDF captures the maximum amount of “side-way” shape expansion on both sides of  $x$ . In Figure 2, axes in (b,c) are inscribed axes of  $x$  and attaining the EDF  $\tilde{R}(x)$ , which is the sum of the geodesic distance between  $x$  to the top-left end of the medial axis  $y$  and  $R(y)$ . The EDF can be understood as the half-length of the longest tube that can be centered at  $x$ .

The extended medial axis is the loci where the inscribed axis cannot be further expanded:

**Definition 4** An axis  $f$  is called maximal if both of its ends are constrained. A point  $x \in M$  lies on the extended medial axis (EMA)  $\tilde{M}$  if every inscribed axis of  $x$  is maximal.

Note that all inscribed axes of an EMA point need to be maximal. This requirement is important for distinguishing the center of the shape from the local symmetry centers. For example, even though the axis in Figure 2 (c) is an inscribed axis of  $x$  and is maximal,  $x$  has some other inscribed axis that is not maximal (e.g., (b)), and hence  $x \notin \tilde{M}$ . On the other hand, the point  $x$  in (d) is on  $\tilde{M}$  since all its inscribed axes are maximal (one is shown in the picture). Observe that  $x$  in (d) is more “centered” with respect to the entire shape than the  $x$  in (c), the latter being centered only with respect to two symmetric shape parts.

We make a final note of the scenario in which the radius  $r_f(x)$  is infinity, which happens when  $f$  is a non-simple path that travels infinitely on both sides of  $x$ . By the above definitions, both ends of  $f$  are constrained, hence  $f$  is maximal. On the other hand,  $\tilde{R}(x) = \infty = r_f(x)$ , hence  $f$  is an inscribed axis of  $x$ , and all inscribed axes of  $x$  have infinite radius. As a result,  $x$  is on the EMA  $\tilde{M}$ , since all its inscribed, infinite-radius axes are maximal.

### 3.3. Properties

EDF and EMA, defined on the medial axis, share several important properties as the boundary distance function and medial axis, which we examine in this section (the proofs are provided in Appendix A,B,C).

We start by examining the range of values of EDF, showing that it is lower bounded by the boundary distance function and is finite away from loops in the medial axes:

**Proposition 1** Let  $x \in M$ :

- (i)  $\tilde{R}(x) \geq R(x)$ , and the equality holds only when  $x \in \partial M$ .
- (ii)  $\tilde{R}(x) = \infty$  iff there is some subset  $S \subset M$  containing  $x$  such that  $\partial S = \emptyset$ .

The result in (i) aligns with the intuition that the “side-way” expansion of the shape around  $x$  (captured by  $\tilde{R}(x)$ ) is no smaller than the uniform expansion there (captured by  $R(x)$ ). An immediate corollary of (ii) is that  $\tilde{R}$  is finite everywhere on the medial axis  $M$  of a simply connected shape  $O$  (i.e., one without interior holes), since  $M$  is a tree and so is any of its subset. If  $O$  contains interior holes, the proposition implies that  $\tilde{R}(x)$  is infinite over the largest subset of  $M$  that does not have open boundaries (similar to the 1-core of a graph), and finite everywhere else.

Next, we examine the local behavior of EDF, and show that the EDF behaves like a geodesic function over the medial axis, similar to the boundary distance function over the 2D shape. We consider the local behavior separately at the boundary of the medial axis, on the EMA, and on the rest of the medial axis:

**Proposition 2** Let  $x \in M$ :

- (i) If  $x \in \partial M$ ,  $\tilde{R}$  has a directional gradient of 1 along  $M$  leaving  $x$ .
- (ii) If  $x \notin \partial M$  and  $x \notin \tilde{M}$ ,  $\tilde{R}(x)$  has a directional gradient of 1 on exactly one of the out-going branches of  $M$  at  $x$ , and a directional gradient of -1 on one or more of the out-going branches.
- (iii) If  $x \in M$  and  $\tilde{R}(x) \neq \infty$ ,  $\tilde{R}(x)$  has a directional gradient of -1 on two or more of the out-going branches at  $x$ .
- (iv) If  $x \in \tilde{M}$  and  $\tilde{R}(x) = \infty$ ,  $\tilde{R}$  is infinite on two or more of the out-going branches at  $x$ .
- (v) In all three cases (ii,iii,iv),  $\tilde{R}$  on the remaining out-going branches are bounded strictly below  $\tilde{R}(x)$ , and have constant gradient -1.

In short, any point on the medial axis that is not a boundary or part of the EMA has some neighborhood where EDF is continuous and has constant gradient of 1. As immediate corollaries, the function  $\tilde{R}$  is upper semi-continuous over all  $M$ , has no local minima except at the boundary  $\partial M$ , and is locally maximal at each point on  $\tilde{M}$  where  $\tilde{R}$  is finite. The last statement also implies that the part of  $\tilde{M}$  where  $\tilde{R}$  is finite consists of isolated points.

Finally, we show that the EMA preserves the topology of the medial axis, which in turn preserves the topology of the 2D shape:

**Proposition 3**  $\tilde{M}$  is homotopy equivalent to  $M$ .

If the shape  $O$  is simply connected, the proposition implies that  $\tilde{M}$  has the homotopy of a point. Combined with

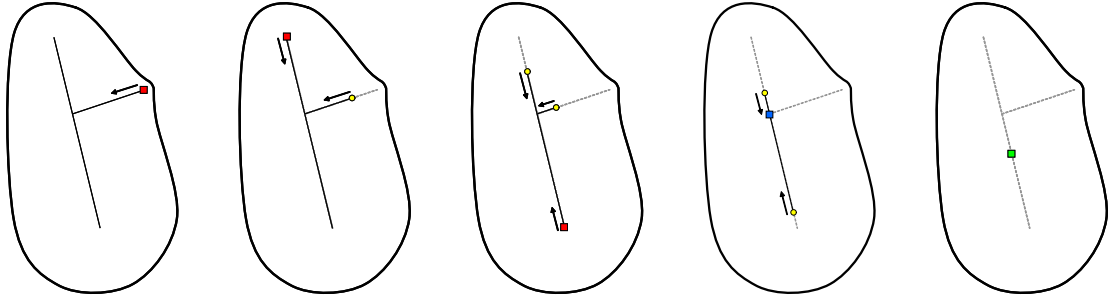


Fig. 3. An illustration of intermediate states in the extended grassfire burning on the medial axis. Yellow dots are the fire fronts, arrows indicate the burning direction, and the red, blue, and green squares are where fire fronts are ignited, annihilated, and quenched.

the argument above that  $\tilde{M}$  consists of only isolated points, one can conclude that  $\tilde{M}$  is a unique point on the medial axis (e.g., a *center point*). If  $O$  contains interior holes,  $\tilde{M}$  has the homotopy of a system of loops. Hence  $\tilde{M}$  consists entirely of the part of  $M$  where  $\tilde{R} = \infty$  without additional isolated points.

#### 4. A grassfire analogy for computation

While explicitly defined, the EDF and EMA cannot be directly computed from their definitions, which involve exploring an infinite set of axes at each point. On the other hand, the properties of the EDF established by Proposition 2, particularly its lack of local minima and constant gradient, suggests that the function can be obtained by propagating values geodesically along the medial axis from its boundary points. In the following, we design a propagation method for computing EDF and EMA guided by their local properties. The propagation bears close resemblance with (and in some sense “continues”) Blum’s grassfire, and hence is called the *extended grassfire transform*.

##### 4.1. Extended grassfire transform

Akin to Blum’s grassfire analogy, imagine the medial axis  $M$  are made up of a thin thread of grass of the same material. Each end  $z \in \partial M$  is *ignited* at time  $R(z)$ , that is, when Blum’s grassfire reaches there. The fire propagates from those ends geodesically along  $M$  at a uniform speed. When a fire front comes to a junction, it continues onwards if there is exactly one remaining un-burned branch, and *annihilates* if there are two or more branches remaining. When multiple fire fronts meet at a same location, and if there is no remaining un-burned branches, the fire fronts *quench* against each other. The process terminates when no fire front is active. A simple example illustrating this grassfire burning is shown in Figure 3.

In this extended grassfire analogy, the EDF at a point on  $M$  is the time at which the point is burned by the fire, and infinity if the point is never burned. If the shape  $O$  is simply connected, the entire  $M$  will be burned out, and the EMA is the quench site of the fire fronts. Otherwise, if  $O$

contains interior holes, EMA is the remaining un-burned portion of  $M$ .

Note that our extended grassfire can be combined with Blum’s grassfire to a single fire-burning process, since the arrival time of Blum’s grassfire at a medial axis point ( $R(x)$ ) is always earlier than the arrival time of the extended grassfire ( $\tilde{R}(x)$ ). In this combined burning, the fire front starts from the boundary of the shape, quenches along the interior of the medial axis, and continues onto the medial axis from their boundaries.

##### 4.2. Discrete algorithm

The analogy gives rise to a simple, thinning-based algorithm that can compute  $\tilde{R}(x)$  and  $\tilde{M}$  over a discretely represented medial axis  $M$  in time linear to the number of elements in  $M$ . The algorithm assumes that  $M$  is represented as a weighted graph that captures a piece-wise approximation of the medial axis. The graph nodes are vertices on the medial axis, and the weight of an arc between two nodes is the length of the line or curve segment connecting the two vertices. In addition, the distance to the shape boundary is given at each degree-1 node (the “end”) of  $M$ .

The algorithm iteratively reduces the graph  $M$  to compute  $\tilde{R}_i$  at each node  $i$ , which are initialized to be the boundary distance at each degree-1 node and infinity elsewhere. At each iteration, the degree-1 node  $i$  with the smallest  $\tilde{R}_i$  is removed with its incident arc. If the removal exposes a new degree-1 node,  $j$ , then  $\tilde{R}_j$  is updated as the sum of  $\tilde{R}_i$  and the weight of arc  $\{i, j\}$ . Iteration terminates when the graph is reduced to with either a single node or a set of cycles, which are output as the EMA  $\tilde{M}$ .

In our experiments, we compute the discrete medial axis  $M$  as the subset of the Voronoi diagram of points sampled on  $O$ , consisting of the interior Voronoi vertices and their connecting Voronoi arcs. This subset is a provenly good approximation of the 2D medial axis, and converges to the medial axis as the sampling density increases [3].

#### 5. Examples and comparisons

We start with two simple examples in Figure 4 computed using our discrete algorithm. One of the two shapes is sim-

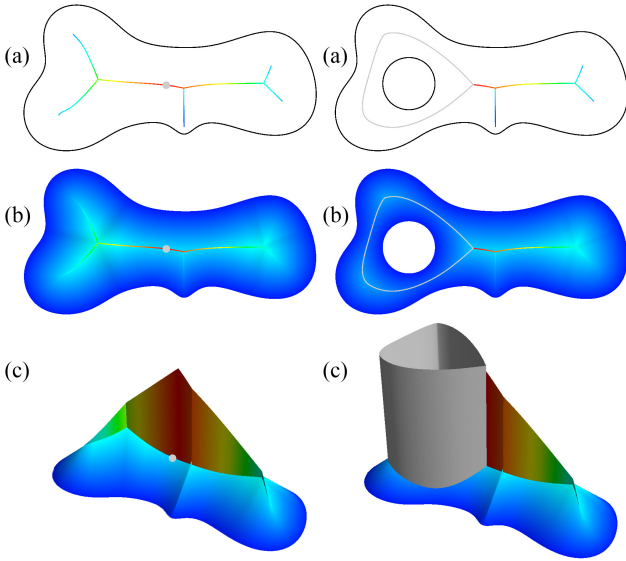


Fig. 4. EDF and EMA in a simply connected shape (left) and a shape with an interior hole (right). The medial axis is colored by the EDF in (a) while the EMA is drawn in black, (b) shows the boundary distance function in the background, and (c) plots both EDF and the boundary distance function as a 3D height map. The heat coloring scheme is used (blue is low and red is high).

ply connected, while the other contains an interior hole. We can observe the properties of the EDF and EMA discussed in Section 3 in this picture. In particular, the EDF is identical with the boundary distance at the ends of the medial axis, and increases at a constant gradient away from the ends (most notably in the 3D height map in (c)) while staying above the boundary distance function (as seen in the overlay in (b)). At each junction, the EDF is continuous along at least two branches. The EMA is the global maximum of EDF in the simply connected shape (the gray dot), and a loop on the medial axis in the other shape (the gray loop) where the EDF is infinite.

Observe from Figure 4 that the medial axis points with higher values of EDF lie in more elongated parts of the shape. The infinite EDF over a medial axis loop describes an infinite elongation there, since a tube can wrap around the loop for infinitely many times. More importantly, observe that EDF is not sensitive to minor boundary perturbations in elongated shape parts. Intuitively, the EDF captures the half-length of a longest fitting tube, which is a global measure that does not change significantly by small protrusions.

The noise-insensitivity of EDF is most notable in a complex example like the one in Figure 5, which contains a significant amount of boundary noise. Observe that the EDF along medial axis branches corresponding to small boundary noise are very close to the boundary distance function (which is most notable in the overlaying picture in (b)), whereas branches corresponding to prominent shape protrusions have much higher EDF than the boundary distance function. Intuitively, EDF and boundary distance at a medial axis point capture respectively the “length” and

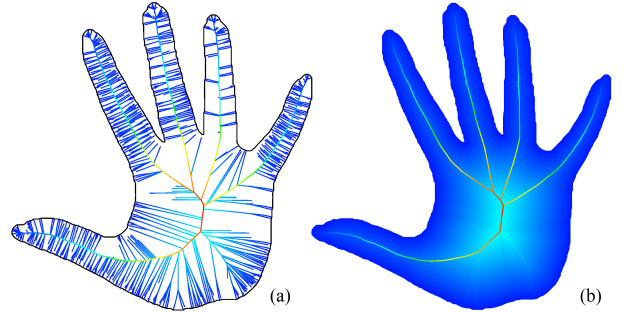


Fig. 5. EDF (a) and overlayed on the boundary distance function (b) for a shape with boundary noise.

“thickness” of the local shape, and hence their difference is a good measure of how protruded the shape is. In fact, this measure has been widely used for identifying significant parts of the medial axes, although without an explicit formulation (see discussion below).

We further examine the stability of EDF and EMA under synthetic boundary perturbations in Figure 6 (top row). Here we perform a uniform perturbation of a square shape (a,b) and a non-uniform perturbation on one side of a key shape (c,d). Note that neither EDF nor EMA changes significantly, despite the change in the topology of the medial axis near the EMA (b) and the addition of a significant amount of medial axis branches (d).

We next compare EDF with two existing global measures on the medial axis, one based on heuristics (the Erosion Thickness) and the other formulated mathematically (the Potential Residue). In the first case, we show that the measure behaves similarly as EDF by giving an explicit characterization of the measure. In the second case, we demonstrate several advantages of EDF in terms of analytical property and stability.

### 5.1. Erosion Thickness

The Erosion Thickness (ET) measure captures the loss of the shape due to the pruning of a medial axis branch. For a point  $x$  located on a medial axis branch directly connected to an end of the medial axis  $y$ , ET is formulated as:

$$ET(x) = d(x, y) + R(y) - R(x)$$

Shaked and Bruckstein [15] proposed an extension of the measure to the entire medial axis using a *rate pruning paradigm*, where  $ET(x)$  is determined as the time at which the pruning front reaches  $x$ . In this paradigm, the pruning front propagates similarly to the fire fronts in our extended grassfire analogy, with two differences. First, the pruning fronts start simultaneously from all medial axis ends at time 0. Second, the pruning front propagates at a non-uniform speed  $1/(1 - R_\alpha(x))$ , where  $R_\alpha(x)$  is the gradient of  $R$  at  $x$ .

While the rate pruning paradigm can be implemented in a discrete algorithm (just like the extended grassfire), an explicit formulation of  $ET(x)$  is not known. As a consequence, the meaning of  $ET(x)$  beyond the medial axis

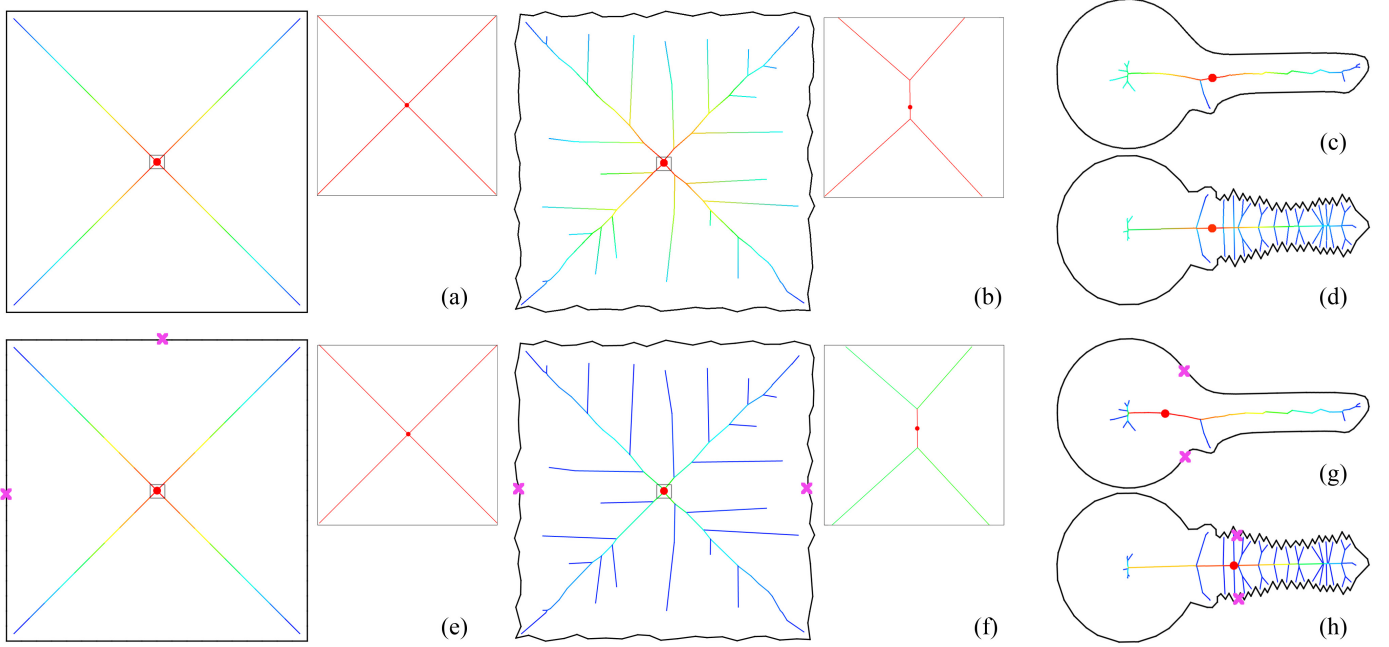


Fig. 6. Comparing EDF (top row) and the Potential Residue (PR) measure (bottom row) on the medial axis under boundary perturbation: the EDF and EMA is stable under both uniform (a,b) and non-uniform (c,d) perturbations, while PR can have sudden jumps (e,f), and both PR and its local maximum can exhibit significant drift (g,h). Each picture is colored by the EDF or PR normalized by the maximum value of EDF or PR present on the medial axis. The inserts in (a,b,e,f) zoom in on the middle of the medial axis where there is a connectivity change after perturbation. The closest boundary points to the local maximum of PR are shown as crosses.

branches directly connected to the ends is not clear. Here we give an explicit definition of  $ET(x)$ , which reveals its link to shape properties. In fact, ET is the residue of EDF after subtracting the boundary distance function, that is,

$$ET(x) = \tilde{R}(x) - R(x)$$

This equivalence of this definition and the pruning time of the rate pruning paradigm can be verified by examining the property of the residue based on those of  $\tilde{R}(x)$  (as discussed in Section 3) and  $R(x)$  (i.e., continuous over  $M$  and has bounded derivative within  $(-1, 1)$ ). As mentioned earlier, the difference of EDF and the boundary distance captures how much “longer” the shape is over its “thickness” around a medial axis point. As a result, medial axis points with higher ET values represent more prominent shape protrusions.

The definition of ET implies that it has very similar behavior as EDF. In particular, both functions share the same continuity and gradient direction over the entire medial axes. Also, both ET and EDF share the same set of local maxima, the EMA. From the practical point of view, the definition offers a simpler way of computing ET: rather than using the original rate pruning paradigm in [15] which requires a pruning rate that varies with a differential quantity ( $R_\alpha$ ), ET can be equally obtained by a uniform-speed propagation (which gives  $\tilde{R}(x)$ ) followed by subtraction of  $R(x)$ .

## 5.2. Potential Residue

The Potential Residue (PR) measures, at each medial axis point  $x$  of a simply connected shape, the shortest distance along the shape boundary between the two boundary points closest to  $x$  [12]. The intuition is that the closest boundary points for medial axis branches reaching to small boundary bumps are typically close together, hence PR is small on those branches. Ogniewicz and Ilg showed that PR increases monotonically from the ends of the medial axis inward, and that there exists a unique local maximum of PR on the medial axis [12]. Note that the recently introduced definition of the curve skeleton of a 3D shape by Dey and Sun [5] is in fact a 3D extension of the local maximum of the PR measure. The extended measure, called the Medial Geodesic Function (MGF), is the geodesic distance on the boundary surface between the two closest boundary points to a medial axis point.

We show several notable differences between EDF and PR through analysis and experiments. First, although being monotonic like EDF, PR in general is not continuous at the junctions of the medial axis, which have three or more closest boundary points. In contrast, EDF is continuous along at least two branches at any junction.

Second, and more importantly, PR and its local maxima can change dramatically under boundary perturbations. We perform the same perturbation tests we had for EDF in Figure 6 for PR (bottom row). Observe that a slight change in the connectivity in the middle of the medial axis (see insert of (f)) causes a big increase in PR there after

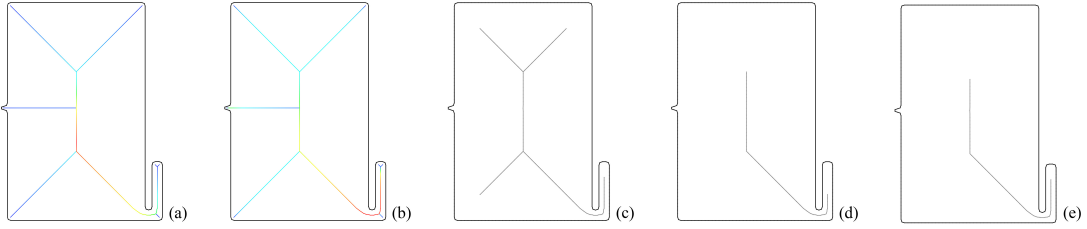


Fig. 7. The Erosion Thickness (ET) measure (a) and Shape Tubularity (ST) measure (b) over a 2D shape, and pruning using a low ET threshold (c), a high ET threshold (d), and the combination of a low ET threshold with a ST threshold (e).

perturbation (note that the coloring of PR in both (e,f) is after normalization by the maximum PR over each medial axis). This is because the pair of closest boundary points to that part of the medial axis (shown as cross marks) change dramatically after perturbation. Also, both PR and its local maxima are strongly affected by non-uniform boundary perturbations. In (g,h), perturbations on one part of the key shape cause PR and its local maximum to shift significantly towards that part, where the curve lengths increase greatly. Note that EDF and EMA are much more stable in both examples.

## 6. Utility

As demonstrated above, EDF offers stable, global measures of shape elongations, and EMA is a stable choice of shape center (for a simply connected shape). In this section, we show several ways that these descriptors can be utilized for shape modeling.

### 6.1. Pruning medial axes

Since meaningful parts of the medial axis should capture elongated shape parts, we can use EDF to define significance measures for pruning the medial axis. As shown in Section 5.1, the difference between EDF and the boundary distance function is equivalent to the Erosion Thickness (ET) measure. Here we present another EDF-based measure called *Shape Tubularity* (ST), defined as:

$$ST(x) = \frac{\tilde{R}(x) - R(x)}{\tilde{R}(x)} = 1 - \frac{R(x)}{\tilde{R}(x)}$$

The measure is a scalar between  $[0, 1]$ , reaching 0 only at the boundary of the medial axis (where  $\tilde{R}(x) = R(x)$ ) and 1 only at the EMA of a non-simply-connected shape (where  $\tilde{R}(x) = \infty$ ).

Intuitively, ST captures the ratio (rather than the difference, as in ET) of the “thickness” over the “length” of the shape around a medial axis point. A high ratio implies a “sharply” protrusion (e.g., a needle), while a low ratio indicates a “blunt” one. Figure 7 compares ET (a) with ST (b) in a synthetic shape that contains both blunt (e.g., corners of the rectangles) and sharp (e.g., the smaller rectangle) protrusions. Note that ET treats the medial axis branches reaching diagonally to the corners of the bigger rectangle

as important as those lying centered in the small rectangle. In contrast, ST along the diagonal branches is much lower than in the small rectangle, indicating that the later is a sharper protrusion.

While capturing “sharpness” of protrusion, ST does not reflect the “size” of protrusion, and hence can be high around boundary noise (see the tip of the small bump in Figure 7 (b)). We therefore combine both ET (which captures the scale of protrusion) and ST for pruning, which removes parts of the medial axis representing shape features that are either small in size or weak in sharpness.

The advantage of using this combination over using ET alone is demonstrated in Figure 7 (c,d,e). Note that using ET alone with a low threshold ( $0.05$  of the dimension of the shape in this example) is sufficient for removing branches caused by boundary noise (see (c)), but branches representing blunt features remain (e.g., the diagonal ones). While these branches can be removed using a high ET threshold (see (d)), branches representing sharp features are significantly shortened (e.g., the center axes of the small rectangle). The result in (e) is produced by using the same ET threshold as in (c) in combination with a suitable ST threshold ( $1 - 1/\sqrt{2} \approx 0.3$ ) (that is, a medial axis point has to satisfy *both* ET and ST thresholds to be retained), which removes the diagonal branches but retain the length of the center axes in the small rectangle as in (c).

Note that the subset of the medial axis satisfying both ET and ST thresholds may not preserve the connectivity of the medial axis. For applications that require a topology-preserving curve skeleton, we may need to expand this subset to retain the original topology of the medial axis. This can be easily done by slightly modifying the discrete thinning algorithm presented in Section 4.2. Instead of removing all degree-1 nodes, we shall preserve those with ST and ET values greater than or equal to the given thresholds. Since removing degree-1 nodes preserve the homotopy of the initial medial axis, the remainder after thinning is a topology-preserving subset. We show more examples of combined pruning with topology preservation in Figure 8, all computed using the same sets of thresholds as in Figure 7 (e).

### 6.2. Shape alignment

Aligning two shapes is an important step for matching and recognition. Oftentimes, the first step of alignment is

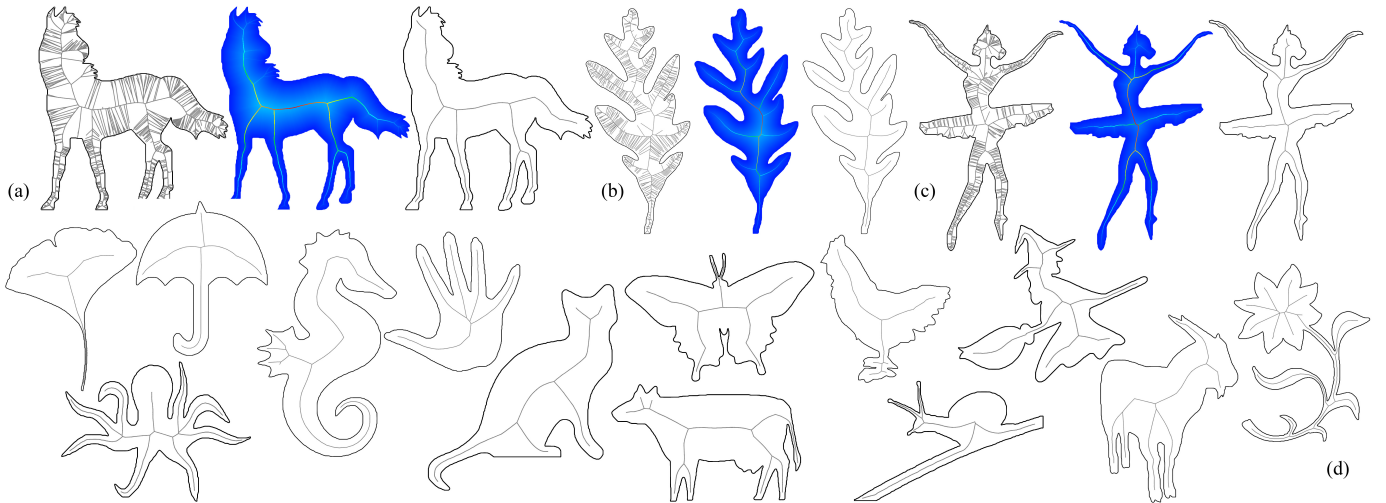


Fig. 8. More pruning examples combining ET and ST. Examples in (a,b,c) include the original medial axes, the EDF and the boundary distance functions, and the pruned medial axes. Only pruned medial axes are shown in (d).

translating two shapes so that their centroid coincide. However, when two shapes that differ by a large variance such as isometric deformations (body movement in a human figure), centroid can often change drastically (e.g., pink dots in Figure 9), and aligning the shape by their centroid would lead to unsatisfactory results (e.g., Figure 9 (b)).

In contrast, EMA, defined by the structure of the medial axes, is stable under a range of deformations including similarity transforms and isometric deformations. Hence EMA offers a good alternative to “centroid” for translational alignment of shapes undergoing these deformations. In the examples on the top of Figure 9, the EMAs are drawn as red dots. Note that they all lie roughly at the waist location of the human body. Alignment using EMA therefore achieves much better overlap between shapes, as shown in (d). We also compare with the local maxima of Potential Residue (PR) measure, which are drawn as blue dots in the pictures. Note that these local maxima can sometimes drift significantly (see the last green figure), a phenomena that we already observed in the previous section. Hence the alignment using the PR local maxima (shown in (c)) does not look as good as the one produced by the EMA.

### 6.3. Shape signature

While EDF offers a global shape metric over the medial axes, many applications such as shape matching require a descriptor (or *signature*) over the boundary of the 2D shape. An ideal boundary signature should not only highlight local geometry, such as concavity or convexity, but also global shape properties, such as shape parts and extremities.

Common boundary signatures include curvature maps and local feature size (LFS), both providing only local shape information. As illustrated in Figure 10, the local curvature is homogenous on most parts of the boundary other than a few places where the curve bends strongly (see (a)).

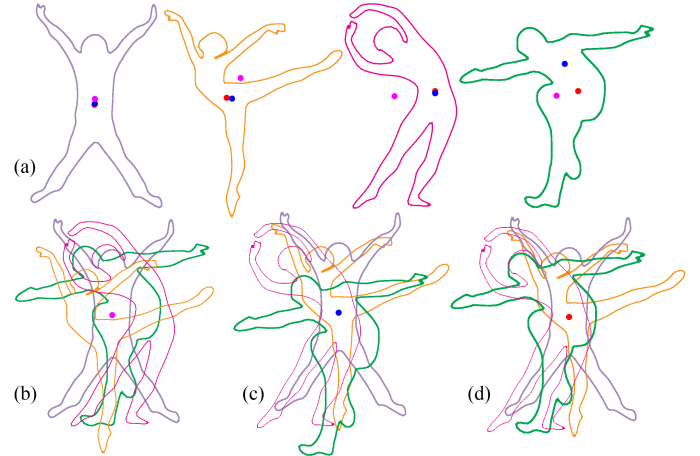


Fig. 9. Top: several human shapes and their centroid (pink), local maximum of PR (blue), and EMA (red). Bottom: alignment using the centroids (b), local maximum of PR (c), and the EMAs (d).

The LFS offers more information as the “thickness” of the local shape, as it measures the distance to the closest medial axis point. But LFS cannot differentiate parts with a common thickness. Also, note that the local nature of these descriptors make them very sensitive to boundary noise.

We introduce a new boundary signature for a simply connected shape, called *Boundary Eccentricity* (BE), which captures how far a boundary point is away from the EMA along the medial axis. For a point  $x$  on the medial axis  $M$ , let  $E(x)$  be the geodesic distance from  $x$  to the EMA. For any boundary point  $p$ , let  $X_p \in M$  be the set of points on the medial axis whose closest boundary point is  $p$ . BE is defined as:

$$BE(p) = \min_{x \in X_p} (E(x) + R(x))$$

Both BE and the function  $E(x)$  over  $M$  are plotted in Figure 10 (c). Observe that, despite the nosiness of the shape, BE is a smoothly varying function that highlights shape parts and extremities that are away from the shape

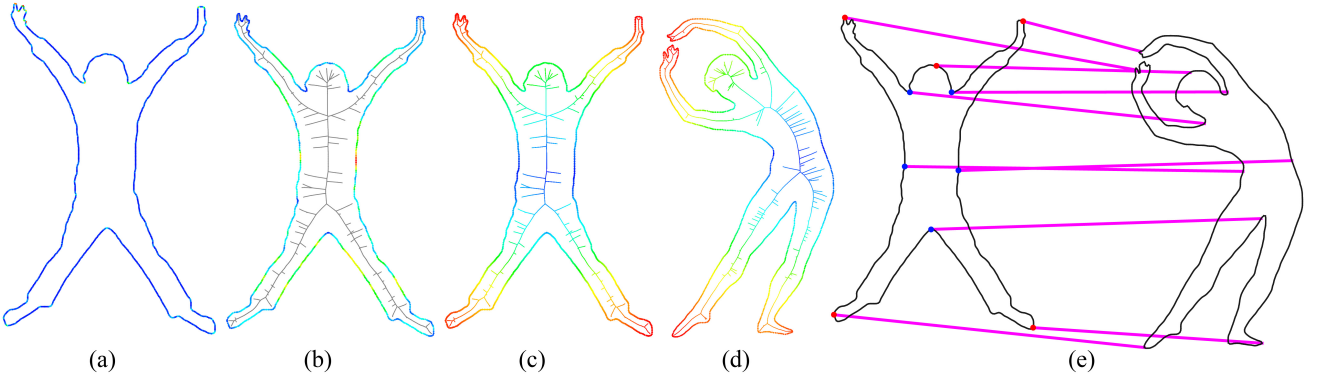


Fig. 10. Boundary signatures: local curvature (a), local feature size (b) showing also the medial axis, Boundary Eccentricity (BE) (c,d) showing also  $E(x)$  over the medial axes, and a matching result using BE (e).

center. As shown in a different shape in (d), BE is also stable under isometric deformations. With these properties, BE is a good descriptor for matching 2D shapes that may be noisy and undergoing large deformations. We demonstrate this by matching the two curves in (c,d) guided by the BE values using a simple dynamic algorithm. The resulting correspondence for several critical points of BE on the first shape (c) is shown in (e).

## 7. Conclusion

In this paper, we define a global shape measure (EDF) over the medial axis that capture shape elongation, a shape center (EMA) where the elongation is maximal, and rigorously study their properties. Both the EDF and EMA can be obtained using an extension of Blum's grassfire analogy onto the medial axis. The EDF and EMA are demonstrated by examples, compared to related formulations, and used in several shape modeling applications.

We have experimentally observed that both EDF and EMA (as well as the Boundary Eccentricity descriptor) are stable under boundary perturbations. As a future work, we would like to theoretically characterize such stability. We are also confident that the work here opens a new path for solving the harder problem in 3D - finding global measures on the 3D medial axis and defining center curves of 3D shapes. Note that the grassfire analogy applies easily to medial axes of 3D shapes. The extended grassfire propagates geodesically from the border of the medial axis sheet at uniform speed. The EDF is the burning time at a medial axis point, and the EMA (the curve skeleton) consists of the quench sites of the fire. This analogy has already led to a simple grid-based thinning algorithm that is capable of extracting significant parts of the 3D medial axis as well as clean curve skeletons [11]. We plan to study explicit mathematical definitions of EDF and EMA in 3D, which will allow us to investigate their theoretical properties and better understand their relation to shape description, as done in 2D in this work.

## Appendix A. Proof of Proposition 1

**Proof:**

- (i) By triangle inequality, for any axes  $f$  containing distinct points  $x, y$ , we have  $R(x) < d_f(x, y) + R(y)$ . Hence  $r_f(x) \geq R(x)$  with the equality attained iff  $x$  is an end of  $f$ . If  $x \in \partial M$ , all axes containing  $x$  will have  $x$  as an end, and hence  $\tilde{R}(x) = R(x)$ . Otherwise, there is some axes that does not have  $x$  as an end, and so  $\tilde{R}(x) > R(x)$ .
- (ii) First, suppose there a subset  $S \subset M$  containing  $x$  such that  $\partial S = \emptyset$ . Then it is possible to obtain an axes  $f$  where  $r_f(x) = \infty$  by extending a path from  $x$  in both directions infinitely without encountering a boundary. Hence  $\tilde{R}(x) = \infty$ .

Next, suppose  $\tilde{R}(x) = \infty$ , which implies  $r_f(x) = \infty$  for some axes  $f$ . Since  $O$  is bounded,  $R$  is finite, and hence both the geodesic distances from  $x$  to both ends of  $f$  need to be infinite. Note that  $O$  is bounded by piece-wise analytic curves, hence  $M$  contains a finite set of analytic curve arcs [4], and so  $M$  does not contain an infinite simple path. As a result, both segments of the axes  $f$  on the two sides of  $x$  need to overlap with themselves. It is easy to see that the subset of  $M$  covered by the segments of  $f$  on each side of  $x$  up to the first overlapping event is one without boundary.

□

## Appendix B. Proof of Proposition 2

We begin by showing several lemmas that lead to the proof.

**Lemma 1** *Extending an axes  $f$  from its ends does not reduce its radius with respect to some fixed  $x \in f$ .*

**Proof:** Denote the ends of  $f$  as  $z_0, z_1$ , and the ends of the extended axes  $f'$  as  $z'_0, z'_1$ . For each  $i \in \{0, 1\}$ , we have:

$$\begin{aligned} d_f(x, z_i) + R(z_i) &= d_{f'}(x, z_i) + R(z_i) \\ &\leq d_{f'}(x, z_i) + d_{f'}(z_i, z'_i) + R(z'_i) \\ &= d_{f'}(x, z'_i) + R(z'_i) \end{aligned}$$

Hence  $r_{f'}(x)$  is no smaller than  $r_f(x)$ .  $\square$

Let  $f$  be an axes containing two points  $x, y$ , we say  $y$  is on the *constrained side* (or *unconstrained side*) of  $x$  if  $y$  lies on the segment of  $f$  between  $x$  and a constrained (or unconstrained) end of  $f$  with respect to  $x$ . We have:

**Lemma 2** Let  $f$  be a non-maximal inscribed axes of  $x \notin \tilde{M}$ , or a maximal axes of  $x \in \tilde{M}$  and  $\tilde{R}(x) \neq \infty$ . The following holds for any  $y \in f$  that lies on the constrained side of  $x$ ,

$$\tilde{R}(y) = \tilde{R}(x) - d_f(x, y)$$

**Proof:** Since  $f$  is an axes containing  $y$ , and since  $y$  is on the constrained side of  $x$ , we have

$$r_f(y) = r_f(x) - d_f(x, y) = \tilde{R}(x) - d_f(x, y).$$

We next show that there exists no other axes  $f'$  such that  $r_{f'}(y) > r_f(y)$ , and hence  $\tilde{R}(y) = r_f(y)$ . Suppose such  $f'$  exists. Denote the two ends of  $f$  as  $z_0, z_1$ , so that  $y$  lies on the segment  $[z_0, x]$  on  $f$ . Denote the two ends of  $f'$  as  $z'_0, z'_1$ , so that the segment  $[y, z'_0]$  on  $f'$  does not share the same half-disk neighborhood of  $y$  as the segment  $[y, x]$  on  $f$  (see Figure B.1 (a)). Consider a new axes  $f''$  made up by segments  $[z'_0, y]$  on  $f'$  and  $[y, z_1]$  on  $f$ . Note that  $x \in f''$ , and

$$\begin{aligned} d_{f''}(x, z'_0) + R(z'_0) &= d_f(x, y) + d_{f'}(y, z'_0) + R(z'_0) \\ &\geq d_f(x, y) + r_{f'}(y) \\ &> d_f(x, y) + r_f(y) = r_f(x) \end{aligned} \quad (\text{B.1})$$

On the other hand,

$$d_{f''}(x, z_1) + R(z_1) = d_f(x, z_1) + R(z_1) \geq r_f(x) \quad (\text{B.2})$$

If the last equality in Equation B.2 holds,  $f$  is a maximal axes of  $x$  whereas  $f''$  is an inscribed axes of  $x$  (because of the strict inequality in Equation B.1), which contradicts to the assumption of the lemma. Otherwise,  $f''$  has a greater radius than  $f$  with respect to  $x$ , which contradicts with the fact that  $f$  is inscribed.  $\square$

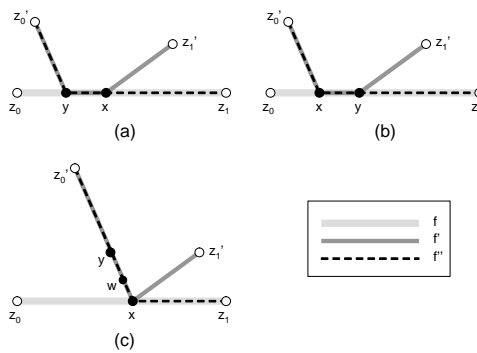


Fig. B.1. Notations used in the proofs.

Let us further denote a *junction* of a set of curves as a point whose local neighborhood on the set contains more

than two 1-D half-disks. We have a similar result as the previous lemma but concerning the unconstrained side of an axes:

**Lemma 3** Let  $f$  be an inscribed, non-maximal axes of  $x \notin \tilde{M}$ . The following holds for any  $y \in f$  that lies on the unconstrained side of  $x$ ,

$$\tilde{R}(y) = \tilde{R}(x) + d_f(x, y),$$

if the half-open interval  $(x, y]$  does not contain any junction on  $M$ , and if

$$d_f(x, y) < \frac{\|d_f(x, z_0) + R(z_0) - d_f(x, z_1) - R(z_1)\|}{2} \quad (\text{B.3})$$

where  $z_0, z_1$  are the two ends of  $f$ .

**Proof:** Using Lemma 2, we only need to show that  $f$  is an inscribed axes of  $y$ , is not maximal, and  $x$  lies on the constrained side of  $y$  on  $f$ . The last two properties are assured by the inequality in Equation B.3, which also implies that  $r_f(y) = r_f(x) + d_f(x, y)$ .

To show inscribedness, suppose on the contrary there exists  $f'$  containing  $y$  such that  $r_{f'}(y) > r_f(y)$ . Since the segment  $(x, y]$  of  $f$  is free of junctions on  $M$ , and since we can always extend an axes without reducing its radius by Lemma 1, we can always find an  $f'$  that shares the segment  $(x, y]$  with  $f$ , and hence  $x \in f'$ . Denote the two ends of  $f$  as  $z_0, z_1$ , so that  $y$  lies on the segment  $[x, z_1]$  on  $f$ . Denote the two ends of  $f'$  as  $z'_0, z'_1$ , so that the segment  $[y, z'_0]$  on  $f'$  contains  $x$  (see Figure B.1 (b)). Consider a new axes  $f''$  made up by segments  $[z'_0, x]$  on  $f'$  and  $[x, z_1]$  on  $f$ . Using a similar argument as in Lemma 2, and since  $f$  is not a maximal axes of  $x$ , one can conclude that  $f''$  has a greater radius than  $f$  with respect to  $x$ , reaching a contradiction with the fact that  $f$  is inscribed.  $\square$

Now we are ready to prove Proposition 2:

**Proof:** We consider each case as follows:

- (i) If  $x \in \partial M$ , any axes  $f$  with one end at  $x$  is an inscribed, non-maximal axes of  $x$  (due to Proposition 1(i)). By Lemma 3, and due to the finite structure of  $M$  [4], there is some finite segment  $[x, y]$  on  $f$  where  $\tilde{R}$  increases with constant gradient 1.
- (ii) If  $x \notin \partial M$  and  $x \notin \tilde{M}$ ,  $x$  has at least one inscribed, non-maximal axes. Note that the unconstrained side of  $x$  in all these axes share the same half-disk neighborhood of  $x$ , or otherwise a longer axes could be constructed by concatenating two unconstrained segments on two inscribed axes. By Lemmas 2 and 3,  $\tilde{R}$  increases with gradient 1 along the shared unconstrained segment, and decreases with gradient -1 along the constrained segment of each inscribed axes.
- (iii) If  $x \in \tilde{M}$  and  $\tilde{R}(x)$  is finite,  $x$  has at least one inscribed axes and all such axes are maximal. By Lemma 2,  $\tilde{R}$  decreases with a gradient of -1 on both sides of each of its inscribed axes.
- (iv) If  $x \in \tilde{M}$  and  $\tilde{R}(x) = \infty$ , by Proposition 1,  $x$  lies in a subset  $S \subset M$  such that  $\partial S = \emptyset$ . Hence all points

on the neighborhood of  $x$  in  $S$  have infinite  $\tilde{R}$ .

- (v) Consider a branch at  $x$  that is not part of any inscribed axes of  $x$ , and take a point  $y$  on the branch so that the segment  $(x, y)$  is free of junctions on  $M$ . Consider an inscribed axes  $f$  of  $x$  and denote its two ends as  $z_0, z_1$  where  $z_1$  is constrained. Consider an inscribed axes  $f'$  of  $y$  and denote its two ends  $z'_0, z'_1$ , so that the segment  $[y, z'_1]$  on  $f'$  contains the segment  $(y, x)$  (see Figure B.1 (c)). Again, such an axes  $f'$  can always be found due to Lemma 1. It is easy to see that the new axes  $f''$  by joining segment  $[z'_0, x]$  on  $f'$  and  $[x, z_1]$  on  $f$  is an inscribed, non-maximal axes of  $y$ , and that

$$d_{f''}(y, x) < \frac{d_{f''}(y, z_1) + R(z_1) - d_{f''}(y, z'_0) - R(z'_0)}{2}.$$

By Lemma 3, for any point  $w$  on the open interval  $(y, x)$ ,  $\tilde{R}(w)$  increases with a constant gradient 1 as  $w$  moves from  $y$  to  $x$ . Combining with the above equation, we have:

$$\begin{aligned} \tilde{R}(w) &= \tilde{R}(y) + d_{f''}(y, w) \\ &< d_{f''}(y, z'_0) + R(z'_0) + d_{f''}(y, x) \\ &< d_{f''}(y, z_1) + R(z_1) - d_{f''}(y, x) \\ &= d_f(x, z_1) + R(z_1) = \tilde{R}(x) \end{aligned}$$

Hence the limit of  $\tilde{R}(w)$  as  $w \rightarrow x$  is bounded below  $\tilde{R}(x)$ .  $\square$

## Appendix C. Proof of Proposition 3

**Proof:** To show homotopy equivalence, we use the common technique of constructing a *deformation retract* from  $M$  to  $\tilde{M}$ . We will find a mapping  $h(t, x)$  that is continuous in both  $t \in [0, t_0]$  for some  $t_0 > 0$  and  $x \in M$ , so that  $h(0, M) = M$  and  $h(t_0, M) = \tilde{M}$ .

We do so by establishing a “direction” field over  $M$  which will be followed by  $h$ . At each point  $x \in M$  that does not belong to  $\tilde{M}$ , Proposition 2 implies that there is a unique out-going branch at  $x$  where  $\tilde{R}$  increases with the gradient of 1. This out-going direction is said to be the *flow direction* at  $x$ ,  $v(x)$ . For  $x \in \tilde{M}$ , its  $v(x)$  is set to null. Note that the flow directions are continuous. By Proposition 2,  $v(y)$  at a point  $y$  in the neighborhood of  $x$  points away from  $x$  only when  $v(x)$  points towards  $y$ , and points towards  $x$  if  $v(x)$  is either null or points away from  $y$ .

We define  $h(t, x)$  as the point on  $M$  that has travelled  $t$  time away from  $x$  at the geodesic speed of 1 following the field  $v$ . By the continuity of  $v$ ,  $h(t, x)$  is continuous in both  $t, x$ . Let  $T = \sup_{x \in M, x \notin \tilde{M}} \tilde{R}(x) + 1$ . Since  $\tilde{R}$  increases at least with the gradient of 1 along  $v$  (with possible jumps at junctions),  $h(T, x)$  for  $x \notin \tilde{M}$  must be at  $\tilde{M}$ , otherwise  $\tilde{R}(h(T, x))$  would be greater than  $\sup_{x \in M, x \notin \tilde{M}} \tilde{R}(x)$ . Since  $h(t, \tilde{M}) = \tilde{M}$  for  $t \in [0, T]$ ,  $h$  is a deformation retract, and  $\tilde{M}$  is homotopy equivalent to  $M$ .  $\square$

## References

- [1] Nina Amenta, Sunghee Choi, and Ravi Krishna Kolluri. The power crust. In *SMA ’01: Proceedings of the sixth ACM symposium on Solid modeling and applications*, pages 249–266, 2001.
- [2] H. Blum. A transformation for extracting new descriptors of form. *Models for the Perception of Speech and Visual Form*, pages 362–80, 1967.
- [3] Jonathan W. Brandt. Convergence and continuity criteria for discrete approximations of the continuous planar skeleton. *CVGIP: Image Underst.*, 59:116–124, January 1994.
- [4] Hyeong In Choi, Sung Woo Choi, and Hwan Pyo Moon. Mathematical theory of medial axis transform. *Pacific J. Math*, 1997.
- [5] Tamal K. Dey and Jian Sun. Defining and computing curve-skeletons with medial geodesic function. In *SGP ’06: Proceedings of the fourth Eurographics symposium on Geometry processing*, pages 143–152, Aire-la-Ville, Switzerland, Switzerland, 2006. Eurographics Association.
- [6] Tamal K. Dey and Wulue Zhao. Approximate medial axis as a voronoi subcomplex. In *SMA ’02: Proceedings of the seventh ACM symposium on Solid modeling and applications*, pages 356–366, 2002.
- [7] Pavel Dimitrov, James N. Damon, and Kaleem Siddiqi. Flux invariants for shape. In *In International Conference on Computer Vision and Pattern Recognition*, pages 835–841, 2003.
- [8] Sandor P. Fekete, Joseph S. B. Mitchell, and Karin Beurer. On the continuous fermat-weber problem. *Oper. Res.*, 53:61–76, January 2005.
- [9] Mark Foskey, Ming C. Lin, and Dinesh Manocha. Efficient computation of a simplified medial axis. *Proceedings of the eighth ACM symposium on Solid modeling and applications*, pages 96–107, 2003.
- [10] W. Lenhart, R. Pollack, J. Sack, R. Seidel, and M. Sharir. Computing the link center of a simple polygon. In *Proceedings of the third annual symposium on Computational geometry*, SCG ’87, pages 1–10, 1987.
- [11] L. Liu, E. Chambers, D. Letscher, and T. Ju. A simple and robust thinning algorithm on cell complexes. *Computer Graphics Forum*, 29(7):2253–2260, 2010.
- [12] R. Ogniewicz and M. Ilg. Voronoi skeletons: Theory and applications. In *Proc. Conf. on Computer Vision and Pattern Recognition*, pages 63–69, 1992.
- [13] R. Pollack, M. Sharir, and G. Rote. Computing the geodesic center of a simple polygon. *Discrete Comput. Geom.*, 4:611–626, September 1989.
- [14] Dennie Reniers, Jarke van Wijk, and Alexandru Telea. Computing multiscale curve and surface skeletons of genus 0 shapes using a global importance measure. *IEEE Transactions on Visualization and Computer Graphics*, 14(2):355–368, 2008.
- [15] Doron Shaked and Alfred M. Bruckstein. Pruning medial axes. *Comput. Vis. Image Underst.*, 69(2):156–169, 1998.
- [16] Kaleem Siddiqi and Stephen M. Pizer. *Medial Representations*. Springer, 2008.
- [17] Avneesh Sud, Mark Foskey, and Dinesh Manocha. Homotopy-preserving medial axis simplification. In *SPM ’05: Proceedings of the 2005 ACM symposium on Solid and physical modeling*, pages 39–50, New York, NY, USA, 2005. ACM.
- [18] F. Wolter. Cut locus and medial axis in global shape interrogation and representation. *Design Laboratory Memorandum 92-2*, MIT, 1993.